RESEARCH ARTICLE

ADVANCED
ELECTRONIC
MATERIALS
Open Access

www.advelectronicmat.de

Check for updates

Improving the Uniformity of Top Emitting Organic Light Emitting Diodes Using a Hybrid Electrode Structure

Mina Riahi, Kou Yoshida, Hassan Hafeez, and Ifor D. W. Samuel*

Some applications of organic light-emitting diodes (OLEDs) require large area, high light output, and high uniformity. It is difficult to achieve these attributes simultaneously because of voltage drops in the contacts, which cannot easily satisfy high optical transparency and electrical conductivity simultaneously. In large area OLEDs, thin electrodes with high sheet resistance induce voltage drops across the devices, leading to non-uniform distribution of light. However, thick electrodes with low sheet resistance decrease the light output due to low transmittance. To overcome this trade-off, a multilayer hybrid electrode based on Ag (20 nm)/WO$_3$/Ag (20 nm)/WO$_3$ is designed to obtain high electrical conductance with low optical loss. Compared to conventional devices using a single Ag (40 nm) top electrode, there is a considerable increase in the external quantum efficiency (EQE) of the device using this electrode (from 11.5% to 25.5% at 1000 cd m^{-2}), while maintaining similar sheet resistance. In addition, a large area ($\approx$57 cm^2) OLED with the hybrid electrode demonstrates a luminance uniformity of 77% as compared to a device using single silver electrode with uniformity of 66%. Therefore, the proposed Ag/WO$_3$/Ag/WO$_3$ hybrid electrode is a promising choice for the fabrication of efficient and uniform large-area OLEDs.

1. Introduction

OLEDs have great potential for applications needing large area bright illumination such as lighting[1–3] and photodynamic therapy.[4–8] However, most research is focussed on individual pixels for displays. Top-emitting OLEDs are attractive and widely used due to their compatibility with various substrates and electrode materials, therefore eliminating the reliance on scarce transparent indium-tin-oxide (ITO) electrodes.[9] A serious limitation encountered when trying to make larger and brighter devices is the voltage loss in the contacts.[10,11] Due to the sheet resistance of the electrodes, the injected current decreases and the light emission distribution becomes non-uniform.[10,12] The voltage drop also leads to a power loss and therefore a decrease in luminous efficacy.[13] Finding electrodes that have higher conductivity whilst maintaining good transmission is essential for development of large area OLEDs that are bright and uniform.

ITO has been widely used as a transparent conductive electrode in bottom emitting devices. Most approaches for improving the conductivity of ITO electrodes are based on using auxiliary metal electrodes.[13–16] Adding a metallic grid in contact with the transparent electrodes can improve the homogeneity of luminescence in bottom emitting OLEDs, but this method leads to loss of light output due to the decreased aperture ratio.[13,14,17] Furthermore, in order to minimise the area of auxiliary electrodes, narrow but thick metal lines are required to achieve high conductivity which is a challenge.[12,15] The organic layers in a device are thinner than the metal grids which can cause a problem of electrical short circuiting between the metal grids and the opposite electrode in devices.[18] Therefore, to prevent shorting, metal lines need to be passivated by an insulator which further lowers the device active area and increases the complexity of the fabrication process.[12] In addition, as the organic layers are soft, adding the grid on top could damage the OLED pixels during the photolithographic patterning process.[19] Thus, this method is mainly applicable to bottom emitting devices.

Using metal nanowire networks is another approach for making transparent conductive electrodes.[20–22] These networks are difficult to make without defects, especially for large area devices.[23] It is possible however to improve the conductivity of metal nanowire electrodes by using large amounts of nanowires, but this also leads to loss of transmittance.[24]

In comparison with nanostructures, silver films can be fabricated defect free in large area OLEDs.[23] Improving conductivity can be achieved by increasing the thickness of the silver film to reduce the sheet resistance.[25] Silver is an attractive candidate to replace ITO due to its higher conductivity (sheet resistance of 20 nm silver film: 3 Ω sq^{-1}) compared to ITO electrode (sheet resistance of 90 nm ITO film : 32 Ω sq^{-1}).[9] However, increasing the thickness of a top silver electrode leads to a reduction

M. Riahi, K. Yoshida, H. Hafeez, I. D. W. Samuel
Organic Semiconductor Centre, SUPA
School of Physics and Astronomy
University of St Andrews
St Andrews KY16 9SS, UK
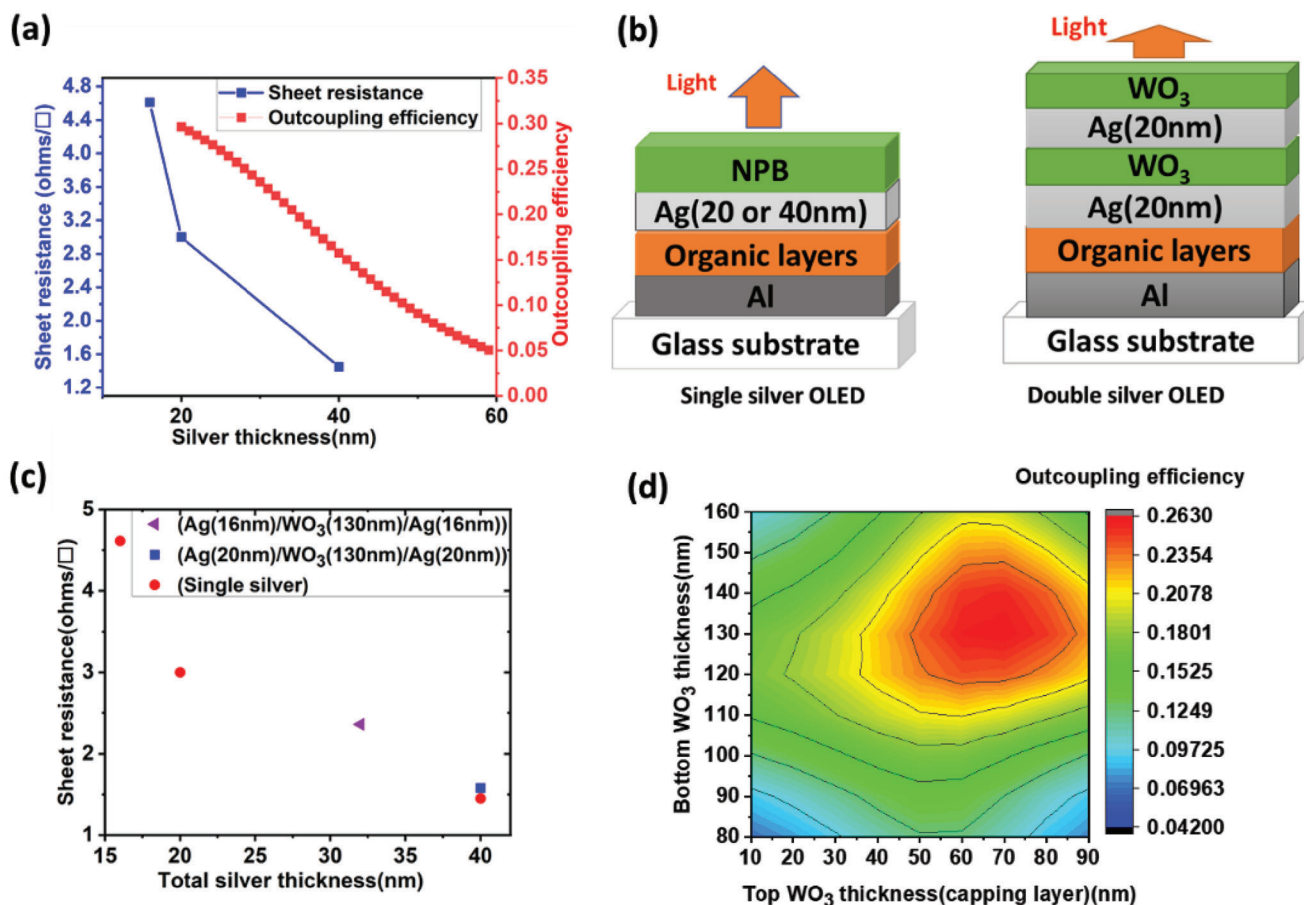E-mail: idws@st-andrews.ac.uk

Figure 1. a) Sheet resistance and outcoupling efficiency as a function of silver thickness. b) Device structure of OLEDs using single silver and multilayer hybrid cathode. c) Sheet resistance measurements of electrodes as a function of total silver thickness for single silver and multilayer hybrid structure. d) Outcoupling efficiency calculation as a function of bottom and top WO_3 thickness for an OLED using the multilayer hybrid electrode.

in transmission and light outcoupling efficiency. This causes a trade-off between optical and electrical properties in metal-based electrodes.

To address this problem, a $WO_3/Ag/WO_3/Ag/WO_3$ structure for the transparent electrode has been proposed, but the red phosphorescent OLED using it only achieved a current efficiency of 6.6 cd A^{-1} at 1000 cd m^{-2}.[26,27] In the present work, we show that the simpler $Ag/WO_3/Ag/WO_3$ structure can enable efficient, large devices, with high uniformity. In the first part of our investigation, we explored and tested the electrode design in small devices with doped charge transport layers. We varied electrode layer thicknesses and demonstrated a considerable improvement in outcoupling efficiency by replacing a single (40 nm) silver layer electrode with a multilayer cathode. Also, we found that the WO_3 layer between silver films can act as a protective layer that prevents the device from being electrically short circuited by the deposition of a thick silver layer.

In addition, as previous studies focused on luminescence uniformity improvement for ITO based OLEDs,[12–17] to the best of our knowledge there is no report on uniformity enhancement for ITO-free large OLEDs. This is a significant gap as ITO is too resistive to use as the only contact in large area devices. We explore the effect of multilayer hybrid electrode on luminescence uniformity in a top-emitting large area OLED. In devices with a single connection to the cathode and anode, driven at 12 mA cm^{-2}, we find that for a single silver electrode the dimmest region is only 21% of the intensity of the brightest region. The hybrid electrode improves this to 47%, and using two contacts to each electrode further improves the uniformity to 77%, making it acceptable for applications such as lighting and photodynamic therapy. The approach mentioned here provides an efficient, and simple solution for the challenges of making uniform top-emitting large area OLEDs.

2. Results and Discussion

2.1. Electrodes Design and Fabrication

To attain highly conductive electrodes, use of a thick metal film is required. **Figure 1**a shows the measured sheet resistance and calculated outcoupling efficiency as a function of silver thickness. 40 nm of silver has a measured sheet resistance of 1.45 Ω sq^{-1} which is nearly half that of 20 nm silver (in the range of 2.9–3.1 Ω sq^{-1}). However, increasing the thickness of metal for the

ADVANCED
SCIENCE NEWS

www.advancedsciencenews.com

**ADVANCED
ELECTRONIC
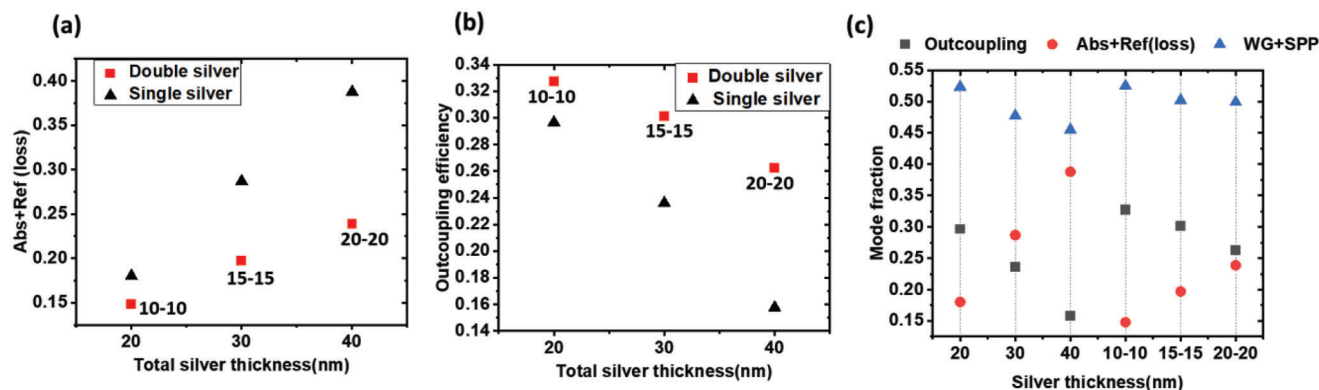MATERIALS**
Open Access

www.advelectronicmat.de

Figure 2. a) Simulated optical loss and b) out coupling efficiency based on total silver thickness to compare single silver and multilayer electrodes. c) Dependence of the optical mode fractions of the devices on the silver thickness. (Thicknesses of WO_3 layers were optimized for each structure. 10-10 denotes $Ag(10\ nm)/WO_3(150\ nm)/Ag(10\ nm)/WO_3(75\ nm)$, 15-15 denotes $Ag(15\ nm)/WO_3(140\ nm)/Ag(15\ nm)/WO_3(70\ nm)$, 20-20 denotes $Ag(20\ nm)/WO_3(130\ nm)/Ag(20\ nm)/WO_3(70\ nm)$.

top electrode leads to a decrease in outcoupling efficiency. For example, the outcoupling efficiency of the silver layer reduces from 30% to 15.7% when the thickness is doubled from 20 to 40 nm. This is due to a reduction in transmittance (Figure S1, Supporting Information). Hence, doubling the silver thickness halves the resistance, but also halves light outcoupling efficiency.

To overcome this trade-off, we used two silver layers connected by WO_3 and optimized the thickness of the WO_3 layer to maximize light extraction. The cross section of the OLEDs using single silver (single silver OLED) and multilayer hybrid electrodes (double silver OLEDs) is illustrated in Figure 1b. The top electrode consists of two 20 nm silver layers separated by WO_3. Figure 1c shows the sheet resistance measurement results for single silver and multilayer electrodes fabricated on a glass substrate. The multilayer electrode using two 20 nm silver layers has a low sheet resistance of $1.58\ \Omega\ sq^{-1}$, which is almost half that of a single 20 nm silver layer. In the multilayer cathode structure, the silver layers act as two parallel resistances to reduce the overall resistance.[26,27]

Contour plots of calculated outcoupling efficiency for the device using the multilayer hybrid electrode as a function of the thickness of the bottom and top WO_3 layers are given in Figure 1d. The top layer of WO_3 acts as a capping layer to enhance the light outcoupling. Light can reflect and transmit at the interface of materials with different refractive indices. The WO_3 layer sandwiched between layers of silver can cause high outcoupling at specific thicknesses as multiple reflections and interferences create constructive interference.[27,28] Therefore, the thickness of WO_3 layers should be optimized to control the interference of light. The thicknesses of WO_3 layers were selected based on the calculation of outcoupling with different thickness of each WO_3 layer. Figure 1d shows the optimized thicknesses for bottom and top WO_3 layers are 130 and 70 nm respectively resulting in outcoupling efficiency of 26.3% which is much higher than our calculation for the same device structure with a single 40 nm silver (15.7%) top electrode. Hence, we calculate that our multilayer electrode achieves much higher light outcoupling efficiency, while providing almost the same sheet resistance.

2.2. Mode Analysis

We performed calculations from the viewpoint of optical mode fractions in order to explain the differences of outcoupling efficiency between the devices using single silver, and multilayer hybrid electrodes when the total thickness of the silver layer in both cases is equal (**Figure 2**). In the calculations, "Abs+Ref loss" denotes the ratio of light with a propagation angle lower than the critical angle of the emission layer/air interface that did not outcouple due to electrode losses (absorption and imperfect reflection) versus total light produced.

Figure 2a shows "Abs+Ref loss" is 0.18 for a single 20 nm silver layer and reduces to 0.14 for the hybrid electrode containing two 10 nm silver layers. For a single 40 nm silver layer, the loss is of 0.38 is reduced to 0.23 for the hybrid electrode containing two 20 nm silver layers. Increasing silver thickness in both cases leads to an increase in amounts of optical losses mainly due to absorption by the metal. However, the double stack structure has substantially lower loss for a given total thickness of silver. Figure 2b illustrates outcoupling efficiency for single silver and hybrid electrodes. For 40 nm total silver thickness, the hybrid electrode gives a large increase in outcoupling efficiency from 0.15 to 0.26. The dependence of the optical mode fractions on the silver thickness estimated from the optical simulations is given in Figure 2c. The fractions waveguide mode (WG) and surface plasmon polariton mode (SPP) mainly depend on total silver thickness rather than single or double stack structure. Therefore, the improvement in outcoupling efficiency by using double stacked silver structure is mainly due to a reduction of absorption loss.

2.3. Electroluminescence Characteristics of OLEDs

We next compare the experimental performance of OLEDs based on three different top electrodes. We fabricated small area red phosphorescent OLEDs with an active area of 4 mm² and compared three contacts: 20, 40 nm single silver, and multilayer structure Ag (20 nm)-WO_3 (130 nm)-Ag (20 nm)-WO_3 (70 nm) for cathodes. **Figure 3**a,b displays current density–voltage –luminance ($J-V-L$) characteristics and EQE as a function of
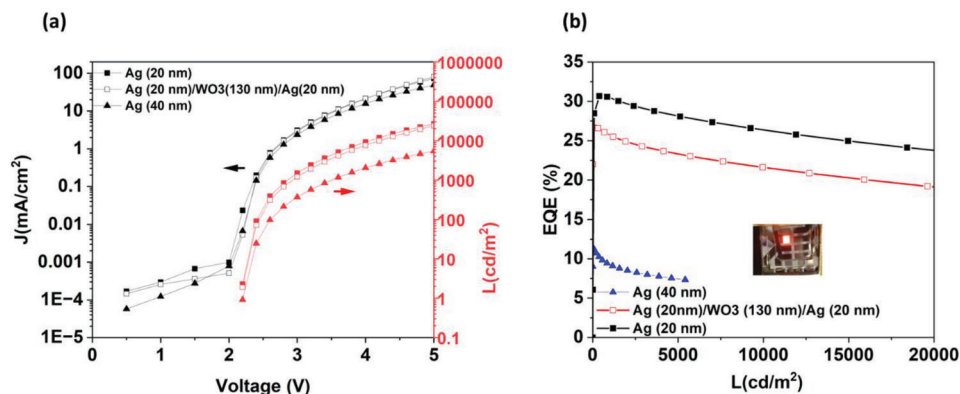
Figure 3. a) Current density−voltage−luminance ($J−V−L$) characteristics of small area (2 mm by 2 mm) OLEDs. b) EQEs of the OLEDs as a function of luminance (L).

luminance for the fabricated devices. The EQE of 20 nm Ag electrode OLEDs was observed to be 30.3% at 1000 cd m^{-2}, however, when the thickness of the silver layer was increased to 40 nm, the EQE considerably dropped to 11.5%. This is in accordance with the aforementioned discussion that increasing the silver layer thickness decreases the outcoupling efficiency and consequently the EQE of the devices. However, when this 40 nm silver thickness was split in two 20 nm silver layers with WO$_3$ layer in between a considerably higher EQE of 25.5% was achieved. This EQE is much closer to that of the thinner device, with the important advantage of a more conductive contact.

2.4. Development of Large Area OLEDs

The next step was to explore how our contact design affected uniformity in a larger device, and so we made large OLEDs of dimensions 7.6 cm by 7.6 cm ($\approx$57 cm^2). Devices with 20 nm single silver and Ag (20 nm)-WO$_3$(130 nm)-Ag (20 nm)-WO$_3$ (70 nm) deliver an irradiance of 5.5 and 4.25 mW cm^{-2} at 25 mA cm^{-2} respectively (**Figure 4**a). It is important to note that large area OLEDs with single thick silver (40 nm) did not work due to being shorted. This can be due to penetration of silver into the organic layers during deposition of the silver. This problem is avoided by

separating the 40 nm silver into two 20 nm silver layers with the WO$_3$ layer in between.

Figure 4b shows electroluminescence spectra of the red phosphorescent OLEDs with 20 nm single silver and multilayer electrodes. The peak wavelength of the emission was at 625 nm for the device with single silver and 612 nm for the device with multilayer hybrid cathode. The difference in the spectra is due to optical interference effects in the multilayer structure.

2.4.1. Luminescence Uniformity Measurement and Simulation

We measured the luminescence homogeneity of the large area OLEDs at 16 points equally spaced over the emitting area using a fibre-coupled charge coupled device camera (fibre-CCD method). In addition, luminescence uniformity was measured for two different conditions for the devices and summarized in **Table 1**. In one case constant current was applied by one contact to the cathode and one contact to the anode (**Figure 5**a), while in the other two cathodes and two anodes were used (**Figure 6**a). Luminescence uniformity was calculated as the ratio of minimum (L_{min}) to maximum EL intensity (L_{max}) over the device area: Luminance uniformity = L_{min}/L_{max}.

Figure 5b illustrates luminescence uniformity measured by the fibre CCD method. When constant current is only applied to
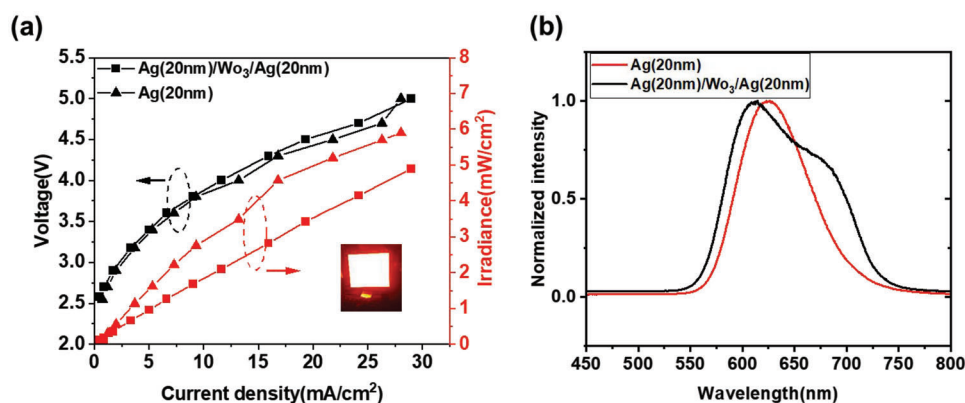

Figure 4. a) $J−V$-irradiance characteristics of large area OLEDs. b) Emission spectrum of OLEDs using single silver and multilayer hybrid cathodes.

Table 1. Comparison of luminescence uniformity of large OLEDs using the hybrid electrode and single silver electrode.

Top electrode structure	Connection	Measured luminescence uniformmit [%]
Ag	One cathode-One anode	21
Ag/WO$_3$/Ag	One cathode-One anode	47
Ag	Two cathodes-Two anodes	66
Ag/WO$_3$/Ag	Two cathodes-Two anodes	77

one cathode-one anode at an average irradiance of 3 mW cm^{-2}, the luminescence uniformity of a large OLED with 20 nm single silver layer for cathode was 21%. The non-uniform light distribution is caused by the sheet resistances of the 20 nm silver top electrode, and the 150 nm Al bottom electrode, measured to be 3 and 0.3 Ω sq^{-1} respectively. Increasing the device size causes voltage drops due to the sheet resistance of the electrodes.[10] Therefore, the injected current decreases, leading to a non-uniform distribution of light. The simulation result in Figure 5c shows that for the device with 20 nm single silver cathode, the current density reduces from 14 to 4.4 mA cm^{-2}.

Figure 5d shows that the luminescence uniformity improves to 47% by using the multilayer electrodes for top cathode. This improvement can be understood from Figure 5e, where the current density can be seen to decrease from 14 to 6.7 mA cm^{-2} for the device using the multilayer electrode. This lower reduction in current density is due to the lower sheet resistance of the top electrode, leading to less variation in light distribution across the device.

The luminescence uniformity results when both cathodes and anodes were employed is displayed in Figure 6. In this case, both single and double silver stack devices showed lower variation of light distribution due to lower reduction in current density. Figure 6b illustrates the luminescence uniformity test measured by the fibre- CCD method. At a current density of 17 mA cm^{-2} and average irradiance of 4.5 mW cm^{-2},
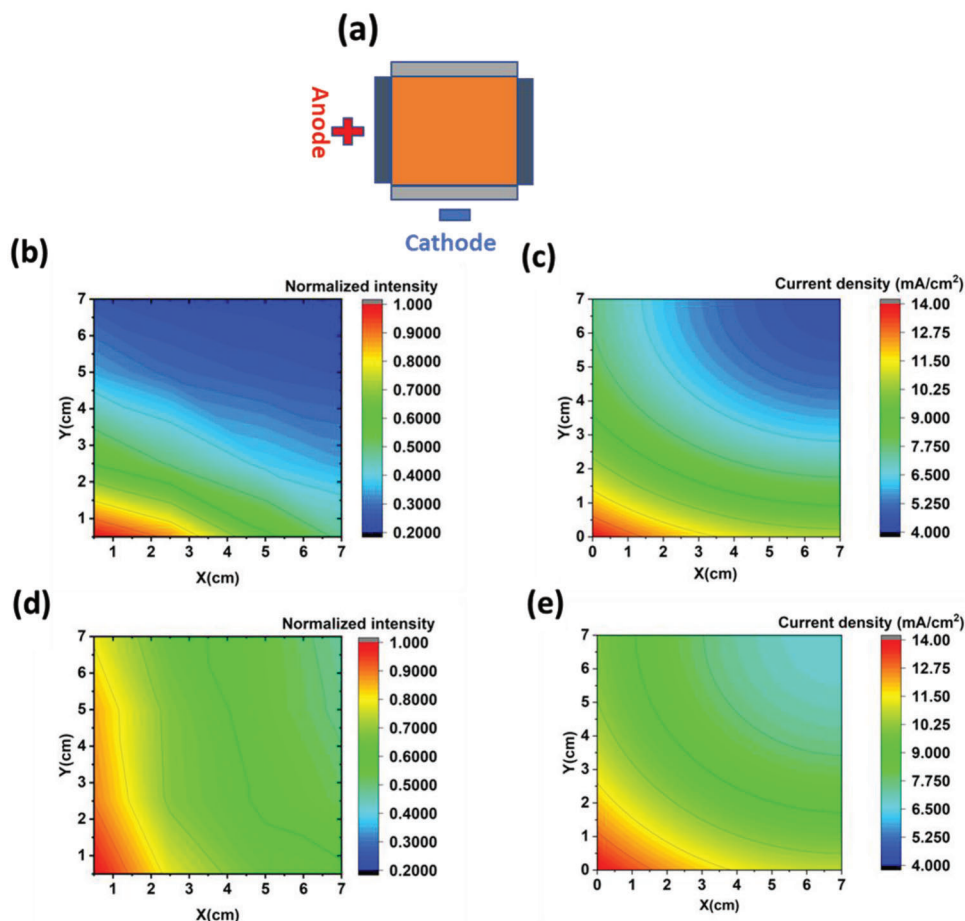

Figure 5. a) Schematic of large OLED using one anode. one cathode. b) Uniformity measurement of OLED using single silver structure for cathode. c) Simulation of current density distribution for large OLED using single silver structure for cathode. d) Uniformity measurement of OLED using multilayer structure for cathode. e) Current density simulation for OLED using multilayer structure cathode.
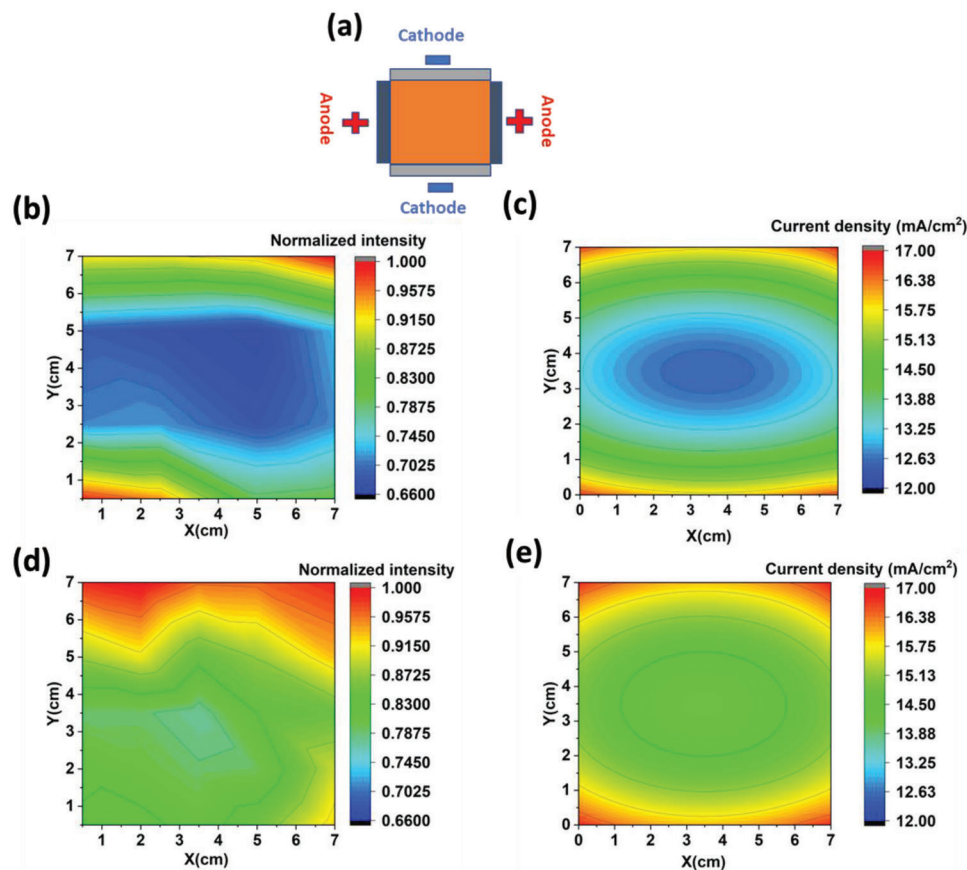
**ADVANCED
SCIENCE NEWS**

www.advancedsciencenews.com

**ADVANCED
ELECTRONIC
MATERIALS**

www.advelectronicmat.de

Figure 6. a) Schematic of large area OLED using two anodes, two cathodes. b) Uniformity measurement of OLED over area using single silver structure for cathode. c) Simulation of current density for large OLED using single silver structure for cathode. d) Uniformity measurement of OLED using multilayer structure for cathode. e) Calculation of current density for OLED using multilayer structure cathode.

the luminescence uniformity of a large OLED (≈ 57 cm^2) with a 20 nm single silver layer cathode was 66%. This is caused by a reduction in current density from 17 to 12.5 mA cm^{-2} (Figure 6c). However, by using the multilayer structure for the cathode, the luminescence uniformity improved to 77% (Figure 6d). Based on the simulation results in Figure 6e the current density reduced from 17 to 14.16 mA cm^{-2} by using the multilayer structure for the cathode. This lower reduction in current density leads to a more uniform emission of light. Measurements of OLED uniformity by a laser beam profiler are provided in supporting information (Figures S4 and S5, Supporting Information).

3. Conclusion

In this work, we introduced the concept of using a multilayer hybrid electrode in a large area top emission OLED to enhance luminescence uniformity. The highly conductive multilayer hybrid electrode reduces the sheet resistance, which is crucial for realizing a large area OLED with uniform distribution of light. Furthermore, separation of a 40 nm silver layer into two 20 nm silver layers in the multilayer hybrid structure leads to a significant improvement in outcoupling efficiency due to reduction in optical loss, whilst maintaining low sheet resistance. This work shows

significant improvement in the trade-off between the optical and electrical properties in devices using ITO free metal electrodes, which will enable the development of applications needing large area and high brightness.

4. Experimental Section

OLED Fabrication: Device fabrication consists of substrate preparation followed by thin film deposition on to the substrate. The glass substrate was ultrasonically cleaned with acetone, and isopropanol for 15 min. After the cleaning process the substrate was transferred into a thermal evaporator (Angstrom Engineering, EVOVAC vacuum deposition system). The chamber of the evaporator was then pumped down to a pressure of 3×10^{-7} mbar and 150 nm aluminium anode was deposited on a cleaned glass substrate at rate of 3 Å s^{-1} using the thermal evaporator at a base pressure of 3×10^{-7} mbar. A 40 nm hole transport layer (HTL) of 2,2′,7,7′-tetra (N, N-di-p-tolyl) amino-9,9-spirobifluorene (Spiro-TTB) was p doped by 2,2-(-(perfluoronaphthalene-2,6-diylidene) dimalononitrile (F6-TCNNQ) (4 wt%) and was deposited at 0.6 Å s^{-1}. A 10 nm electron-blocking layer of NPB (*N,N*′-bis (naphthalen-1-yl)-*N,N*′-bis(phenyl)-benzidine) was deposited at 0.3 Å s^{-1}. The emission layer (40 nm thick) consisted of (2-methyldibenzo[f,h]quinoxaline)(acetylacetonate)iridium(III) Ir(MDQ)$_2$(acac) at (10 wt%) in a NPB host. A 10 nm hole blocking layer bis(8-hydroxy-2-methylquinoline)-(4-phenylphenoxy) aluminium

(BAlq) was deposited at 0.3 Å s^{-1}. A 60 nm electron transport layer of 4,7-diphenyl-1,10- phenanthroline (BPhen) was doped by Cs and deposited at 1 Å s^{-1}.

For devices using single silver electrode, 20 and 40 nm Ag were deposited at 1 Å s^{-1} and an 80 nm NPB capping layer was deposited at 0.6 Å s^{-1}. For the multilayer top electrode, the structure of Ag (20 nm)-WO$_3$-Ag (20 nm)-WO$_3$ was used. Semi-transparent silver layers and WO$_3$ were deposited at 1 and 0.6 Å s^{-1} respectively. After evaporation the fabricated OLEDs inside a nitrogen glovebox were encapsulated by using encapsulation glass, UV-curable epoxy glue, and a moisture getter.

OLED Characterization: The electrical characteristics of the small area OLEDs were measured using a source measurement unit (Keithley 2400, Keithley) to scan the devices with constant voltage. The optical characteristics were measured with a multimeter (Keithley 2000, Keithley) and a calibrated Si photodiode. External quantum efficiency (EQE) calculations were performed based on the assumption that the emission profiles of the OLEDs are Lambertian.

For characterization of large area OLEDs, a direct current power supply (PS-305D) was used. The irradiance of OLEDs was measured with an optometer (P9710, Gigahertz Optik). The sheet resistance of electrodes was measured by four-point probe method using multimeter (Keithley 2000).

Luminescence Uniformity Measurement of Large Area OLEDs: Uniformity test and EL spectra of the devices were measured using a spectrograph (MS125, Oriel) coupled to a charge coupled device (CCD) camera (DV420-BU, Andor). Luminance distributions were measured by moving the fibre to different points to measure EL spectra. The intensity was obtained by integrating the spectrum over wavelength. The intensity at different points was normalized to the maximum value to calculate luminescence uniformity. Imaging was performed using a beam profilometer (Lasercam HR from Coherent).

OLED Simulation: Optical simulation of the devices was conducted in Spyder using a custom-made program-based Python programming language. This simulation is based on emission dipole as forced damped harmonic oscillator and embedded in thin film stacks.[29]

Refractive indexes of Ag and WO$_3$ used in optical simulation were measured using spectroscopic ellipsometer (J. A. Woollam VASE).

Calculation of voltage drops for large area OLEDs was performed by solving the second order differential equations[10] based on FDM (finite difference method) using MATLAB (MathWorks). Further details of the OLED simulation are given in supporting information.

Supporting Information

Supporting Information is available from the Wiley Online Library or from the author.

Conflicts of interest

The authors declare no conflict of interest.

Data Availability Statement

The data that support the findings of this study are openly available in PURE at https://doi.org/10.17630/b277eba7-87f5-472f-b459-eb70935e01b7, reference number 286642426.

[1] J. P. Spindler, T. K. Hatwar, *J. Soc. Inf. Disp.* **2009**, *17*, 861.
[2] R. Pode, *Renewable Sustainable Energy Rev.* **2020**, *133*, 110043.
[3] S.-J. Zou, Y. Shen, F.-M. Xie, J.-D. Chen, Y.-Q. Li, J.-X. Tang, *Mater. Chem. Front.* **2020**, *4*, 788.
[4] C. Lian, M. Piksa, K. Yoshida, S. Persheyev, K. J. Pawlik, K. Matczyszyn, I. D. W. Samuel, *Npj Flexible Electron.* **2019**, *3*, 18.
[5] Y. Jeon, I. Noh, Y. C. Seo, J. H. Han, Y. Park, E. H. Cho, K. C. Choi, *ACS Nano* **2020**, *14*, 15688.
[6] S. K. Attili, A. Lesar, A. Mcneill, M. Camacho-Lopez, H. Moseley, S. Ibbotson, I. D. W. Samuel, J. Ferguson, *Br. J. Dermatol.* **2009**, *161*, 170.
[7] M. Piksa, C. Lian, I. C. Samuel, K. J. Pawlik, I. D. W. Samuel, K. Matczyszyn, *Chem. Soc. Rev.* **2023**, *52*, 1697.
[8] F. V. Cabral, C. Lian, S. Persheyev, T. K. Smith, M. S. Ribeiro, I. D. W. Samuel, *Adv. Mater. Technol.* **2021**, *6*, 2100395.
[9] T. Schwab, S. Schubert, S. Hofmann, M. Fröbel, C. Fuchs, M. Thomschke, L. Müller-Meskamp, K. Leo, M. C. Gather, *Adv. Opt. Mater.* **2013**, *1*, 707.
[10] K. Neyts, M. Marescaux, A. U. Nieto, A. Elschner, W. Lövenich, K. Fehse, Q. Huang, K. Walzer, K. Leo, *J. Appl. Phys.* **2006**, *100*, 114513.
[11] J. W. Park, D. C. Shin, S. H. Park, *Semicond. Sci. Technol.* **2011**, *26*, 034002.
[12] M. Janka, E. Saukko, P. Raumonen, D. Lupo, *Org. Electron.* **2014**, *15*, 3431.
[13] J. Park, J. Lee, Y.-Y. Noh, *Org. Electron.* **2012**, *13*, 184.
[14] K. Neyts, A. Real, M. Marescaux, S. Mladenovski, J. Beeckman, *J. Appl. Phys.* **2008**, *103*, 093113.
[15] M. Slawinski, M. Weingarten, M. Heuken, A. Vescan, H. Kalisch, *Org. Electron.* **2013**, *14*, 2387.
[16] J. Park, J. Lee, D. Shin, S. Park, *J. Disp. Technol.* **2009**, *5*, 306.
[17] H. W. Bae, Y. H. Son, B. Y. Kang, J. M. Lee, H. Nam, J. H. Kwon, *Opt. Express* **2015**, *23*, 30701.
[18] S. Jung, S. Lee, M. Song, D.-G. Kim, D. S. You, J.-K. Kim, C Su Kim, T.-M. Kim, K.-H. Kim, J.-J. Kim, J.-W. Kang, *Adv. Energy Mater.* **2014**, *4*, 1300474.
[19] B. Niesen, B. P. Rand, P. Van Dorpe, D. Cheyns, L. Tong, A. Dmitriev, P. Heremans, *Adv. Energy Mater.* **2013**, *3*, 145.
[20] C. H. Liu, X. Yu, *Nanoscale Res. Lett.* **2011**, *6*, 2.
[21] P. Kou, L. Yang, C. Chang, S. He, *Sci. Rep.* **2017**, *7*, 42052.
[22] S. Hu, J. Gu, W. Zhao, H. Ji, X. Ma, J. Wei, M. Li, *Adv. Mater. Technol.* **2019**, *4*, 1900194.
[23] D. Zhao, C. Zhang, H. Kim, L. J. Guo, *Adv. Energy Mater.* **2015**, *5*, 2.
[24] H. Li, Y. Liu, A. Su, J. Wang, Y. Duan, *Sci. Rep.* **2019**, *9*, 17998.
[25] S.-R. Park, M. C. Suh, *Opt. Express* **2018**, *26*, 4979.
[26] J. H. Han, D. Y. Kim, D. Kim, K. C. Choi, *Sci. Rep.* **2016**, *6*, 29341.
[27] J. H. Han, D.-H. Kim, E. G. Jeong, T.-W. Lee, M. K. Lee, J. W. Park, H. Lee, K. C. Choi, *ACS Appl. Mater. Interfaces* **2017**, *9*, 16343.
[28] K. Hong, K. Kim, S. Kim, I. Lee, H. Cho, S. Yoo, Ho W Choi, N.-Y. Lee, Y.-H. Tak, J.-L. Lee, *J. Phys. Chem. C* **2011**, *115*, 3453.
[29] M. Furno, R. Meerheim, S. Hofmann, B. Lüssem, K. Leo, *Phys. Rev. B: Condens. Matter Mater. Phys.* **2012**, *85*, 115205.